Journal of Applied Physics

Determination of electrical properties of degraded mixed ionic conductors: Impedance studies with applied dc voltage

Cite as: J. Appl. Phys. **122**, 244101 (2017); https://doi.org/10.1063/1.5006062
Submitted: 21 September 2017 • Accepted: 20 November 2017 • Published Online: 22 December 2017

T. J. M. Bayer, J. J. Carter, Jian-Jun Wang, et al.

AIP Publishing

Determination of electrical properties of degraded mixed ionic conductors: Impedance studies with applied dc voltage

T. J. M. Bayer,[1,a)] J. J. Carter,[1] Jian-Jun Wang,[1] Andreas Klein,[2] Long-Qing Chen,[1] and C. A. Randall[1]

[1]*Department of Materials Science and Engineering, and Materials Research Institute, The Pennsylvania State University, University Park, Pennsylvania 16802, USA*

[2]*Institute of Materials Science, Surface Science Division, Technische Universität Darmstadt, 64287 Darmstadt, Germany*

(Received 21 September 2017; accepted 20 November 2017; published online 22 December 2017)

Under electrical bias, mixed ionic conductors such as $SrTiO_3$ are characterized by oxygen vacancy migration which leads to resistance degradation. The defect chemistry to describe the relationship between conductivity and oxygen vacancies is usually obtained by high temperature conductivity data or quenching experiments. These techniques can investigate the equilibrated state only. Here, we introduce a new approach using in-situ impedance studies with applied dc voltage to analyze the temperature dependent electrical properties of degraded $SrTiO_3$ single crystals. This procedure is most beneficial since it includes electric field driven effects. The benefits of the approach are highlighted by comparing acceptor doped and undoped $SrTiO_3$. This approach allows the determination of the temperature activation of both anodic and cathodic conductivity of Fe-doped $SrTiO_3$ in the degraded state. The anodic activation energy matches well with the published results, while the activation energy of the degraded cathode region reported here is not in agreement with earlier assumptions. The specific discrepancies of the experimental data and the published defect chemistry are discussed, and a defect chemistry model that includes the strong temperature dependence of the electron conductivity in the cathode region is proposed. *Published by AIP Publishing.*

https://doi.org/10.1063/1.5006062

I. INTRODUCTION

Passive components such as capacitors and piezoelectric actuators utilizing mixed ionic conductors including $BaTiO_3$, $Pb(Zr,Ti)O_3$, and $(K,Na)NbO_3$ are widely used for industrial applications.[1–3] However, performance and lifetime are limited when the devices are exposed to increased temperature and field stress.[4–8] Highly accelerated lifetime tests (HALTs)[4,9–11] are commonly used to determine the mean time to failure and investigate the resistance degradation phenomenon. HALT studies of the model system Fe-doped $SrTiO_3$ identified oxygen vacancy migration as the major cause of changes in resistance.[12] However, recent in-situ impedance studies[13] demonstrated that HALT measurements, which monitor the effective conductivity during resistance degradation are not sufficient to describe the spatio-temporal changes in conductivity. The oxygen vacancy enriched cathode region exhibits a considerably lower electron conductivity than predicted. This finding illustrated that it is particularly unfavorable to rely only on the equilibrium state defect chemistry from quenching,[14–17] high temperature conductivity,[17–20] and bulk polarization[21] experiments, while degradation is caused by an external field stress. It is the aim of this work to introduce an approach to bridge the gap between measurement and simulation by providing temperature dependent electrical properties of the degraded state under field stress.

To determine the electrical properties of the degraded state, it is necessary to degrade the sample and simultaneously obtain the distribution of local conductivity. This is possible with in-situ impedance, since the dc voltage allows degradation while ac frequency sweeps allow the determination of the distribution of conductivity. The determination of local conductivity is mainly built on the relation of conductivity σ, relative permittivity ε_r, permittivity of free space ε_0, and relaxation frequency f_r, which is given as follows:[13,22,23]

$$f_r = \frac{\sigma}{2\pi\varepsilon_0\varepsilon_r}. \tag{1}$$

This relationship applies for a parallel element of a capacitor and resistor that is characterized by a Debye peak centered at f_r when plotted as the imaginary part of the modulus $M''(f)$.[22] If the measured sample exhibits two differently conductive regions positioned in series, two Debye peaks separated in the frequency space can be expected. For degraded Fe-doped $SrTiO_3$, this situation with two considerably different conductive regions is given, and both anode and cathode conductivity can be determined.[13,22] There have been several attempts in the literature to obtain details about the electrical properties of the degraded state.[24,25] However, none of these investigations has taken into account that the degraded state is not stable and oxygen vacancy re-equilibration begins as soon as the electric field is turned off.[13,22,23,26,27] The only viable way to investigate the degraded state is by maintaining the applied dc field.

Figure 1 illustrates the generally accepted dependency of total conductivity on the oxygen vacancy concentration for Fe-doped $SrTiO_3$.[12,18,21,28,29] The total conductivity

a)Author to whom correspondence should be addressed: tjb5774@psu.edu

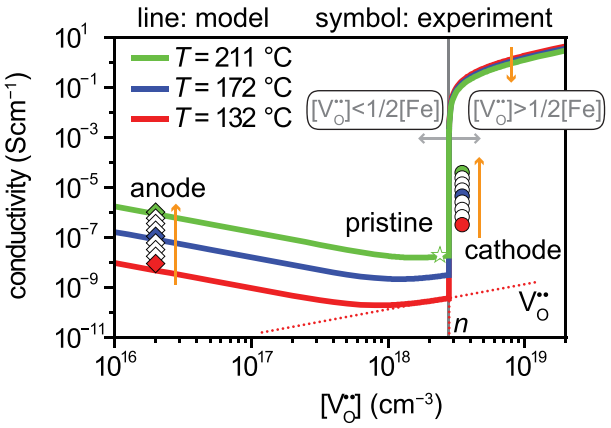

FIG. 1. Plot of conductivity as a function of oxygen vacancy concentration (lines) based on the published defect chemistry of Fe-doped $SrTiO_3$. The symbols indicate the conductivity values of the anodic and cathodic region in the degraded state obtained by the method described in this article. The arrows indicate trends with increasing temperature. The dashed lines show the partial conductivities due to electrons or oxygen vacancies. The model and experiment match in the anodic region, while the experimental results indicate a signifcantly lower conductivity in the cathodic region in comparison to the model.

consists of contributions from electrons n, holes p, and oxygen vacancies $V_o^{\bullet\bullet}$. With increasing oxygen vacancy concentration, the dominant charge carrier species varies from holes via oxygen vacancies to electrons. To reach the pristine state, the samples are quenched in an oxygen partial pressure regime so that oxygen vacancies are the dominant charge carrier and conductivity is low. During resistance degradation, oxygen vacancies migrate to the negatively charged electrode resulting in an oxygen vacancy poor anode region and an oxygen vacancy rich cathode region.[12,29] Local charge compensation results in an increased hole and Fe^{4+} concentration in the anode region, while the electron concentration is increased in the cathode region to compensate the oxygen vacancies.[12,20,28–30] The distinct changes in conductivity are due to the more than seven orders of magnitude higher electron and hole mobility in contrast to the oxygen vacancy mobility. For doped or reduced $SrTiO_3$, both electrons and holes were found to move freely in the conduction and valence band, respectively.[20,31–33] In addition, no trap states were found in the pristine Fe-doped $SrTiO_3$ single crystal.[34] In particular, there is an abrupt increase in conductivity when $[V_o^{\bullet\bullet}] > 1/2[\mathrm{Fe}]$ since the excess oxygen vacancies are not compensated by iron but by electrons. The degraded state is reached once the local electron, hole, Fe^{3+}, Fe^{4+}, and oxygen vacancy concentrations establish an equilibrium state with the local field so that the local conductivity does not change over time. As a consequence, the oxygen vacancy profile is expected to be time invariant due to equilibration of oxygen vacancy drift and diffusion.

Figure 1 also displays the temperature dependent conductivity values of Fe-doped $SrTiO_3$ in the degraded state. The respective concentration of oxygen vacancies in the anode and cathode region is extracted from the simulations.[29] The measured conductivity values for the anode region are in a very good agreement with the published defect chemistry,[21] while considerable discrepancies are observed for the cathode region.[13] Determination of conductivity values and resulting activation energy of differently conductive regions within the samples are introduced and discussed in this article. Undoped and Fe-doped $SrTiO_3$ single crystals are used to illustrate the capabilities of in-situ impedance studies. For the specific case of degraded Fe-doped $SrTiO_3$, a defect model is proposed which is capable of capturing the discrepancies of the observed conductivity in the cathode region.

II. EXPERIMENTAL

Nominally undoped and Fe-doped (0.01 wt. %) $SrTiO_3$ single crystals purchased from MTI Corporation were investigated. The single crystals with dimensions of $3 \times 3 \times 0.5\,\mathrm{mm}^3$ were first annealed in an oxygen partial pressure of 2 Pa at 900 °C. After a sufficient equilibration time of more than 15 h, the crystals were quenched to room temperature to freeze in the established oxygen vacancy concentration. Pt was sputtered on both $3 \times 3\,\mathrm{mm}^2$ surfaces for planar or $0.5 \times 3\,\mathrm{mm}^2$ surfaces for lateral electrodes.

In-situ impedance studies were carried out using an Agilent Precision LCR Meter E4980A. Measurements with 201 data points were taken in the range of 20 Hz to 2 MHz with an ac voltage of 1 V. The performed time schedule of the dc voltage and temperature to obtain the results of this study is shown in Fig. 2. This includes the measurement of the temperature dependence of the pristine condition, the degradation process, and the temperature dependence of the degraded state. First, the pristine state is studied by increasing the temperature stepwise in the absence of a dc voltage. Second, the sample is degraded at a constant temperature and applied dc voltage. The duration of this step depends on the required time to stabilize the degraded state. Third, the dc voltage is kept on to prevent recovery[13,23] and frequency sweeps are performed while the temperature is gradually decreased.

III. RESULTS

The investigation of the degradation process and degraded state of Fe-doped and undoped $SrTiO_3$ is presented in Figs. 3 and 4, respectively. In Sec. III A, important features of the degradation process are discussed, while Sec. III B is focused on the description of the degraded state

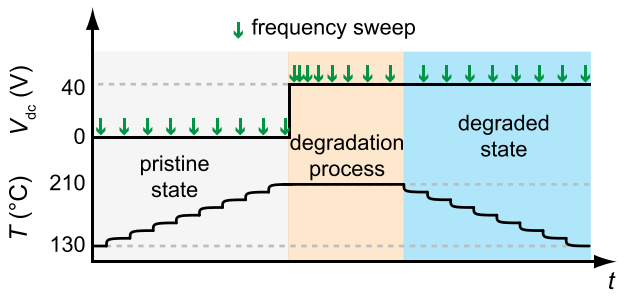

FIG. 2. Time schedule of dc voltage, temperature, and frequency sweeps to investigate the pristine state, the degradation process, and the degraded state.

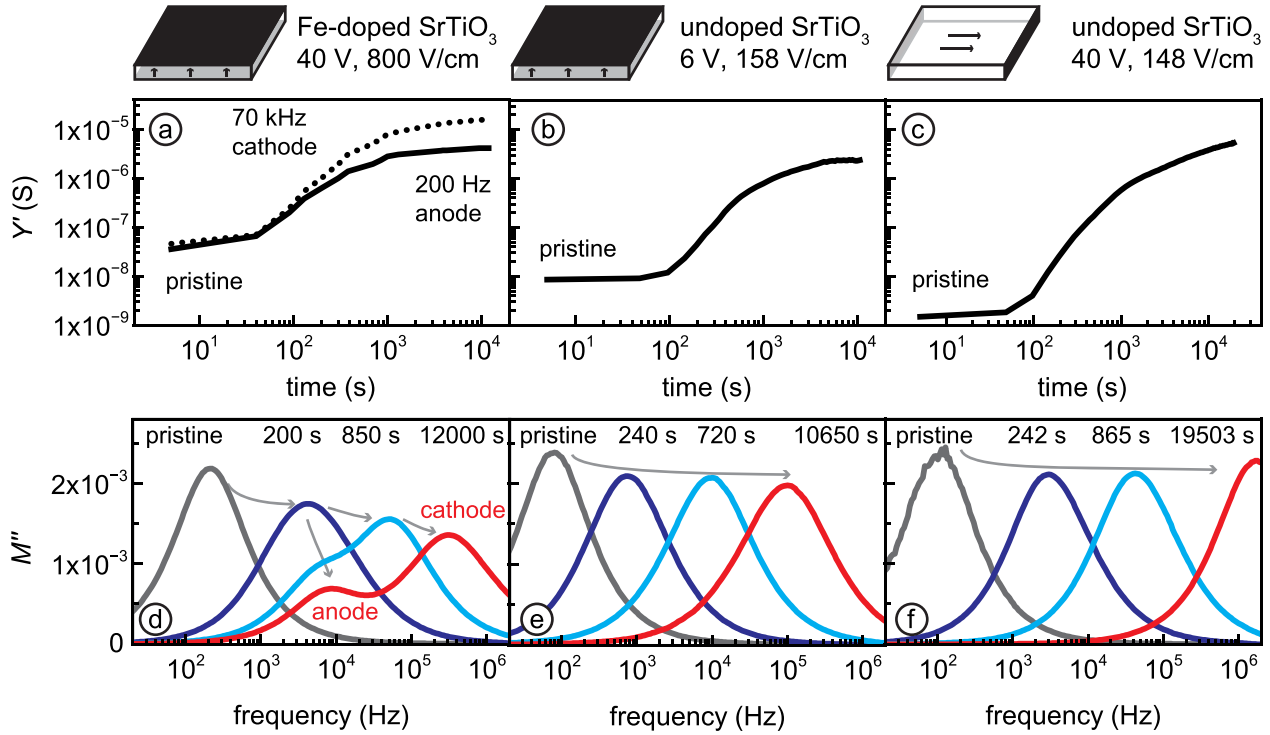

FIG. 3. Degradation of Fe-doped and undoped $SrTiO_3$ in the planar geometry and undoped $SrTiO_3$ in the lateral geometry. Degradation is illustrated as admittance as a function of time at a fixed frequency and as an imaginary part of the modulus M'' as a function of frequency for select times.

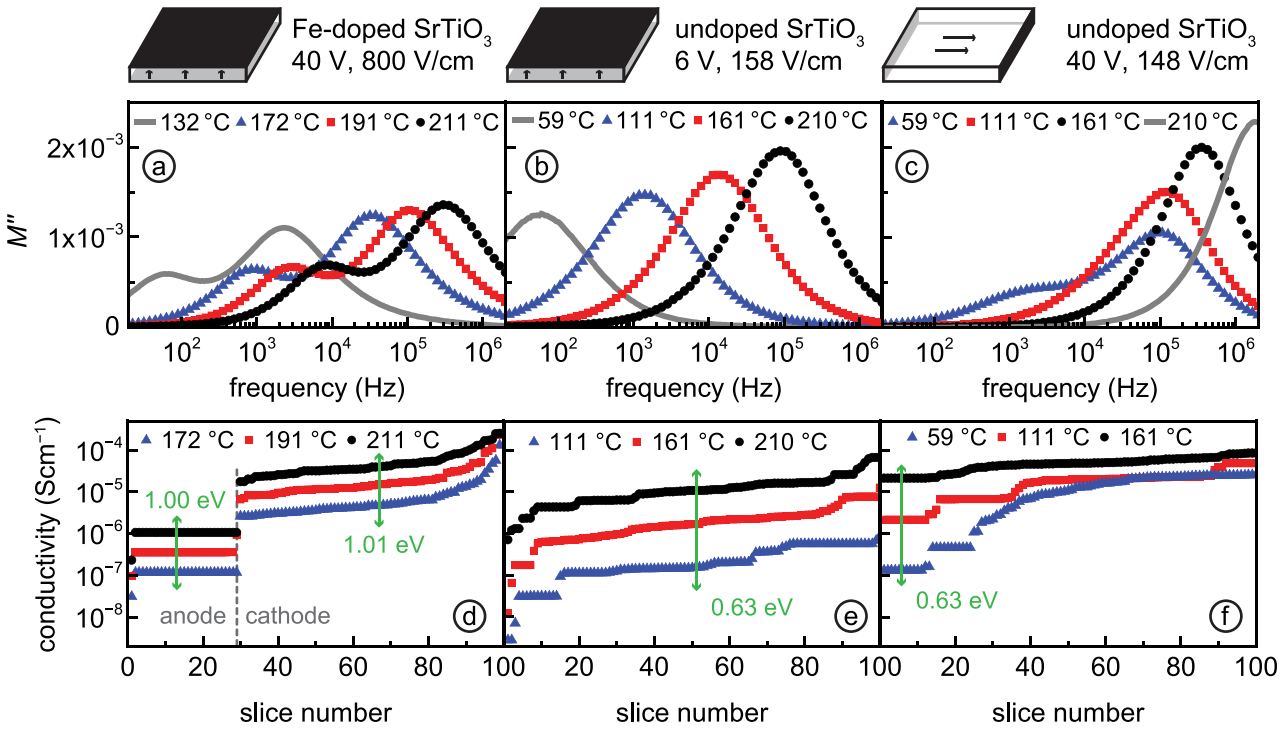

FIG. 4. Temperature dependent electrical properties of degraded $SrTiO_3$ illustrated as modulus spectra and corresponding conductivity distribution for selected temperatures.

as a function of temperature. The impedance response as a function of temperature for the pristine state is not shown here since it is discussed in detail elsewhere.[21,29,35–37] The activation energies of pristine Fe-doped (0.70 eV) and undoped (0.62 eV) $SrTiO_3$ are in accordance with literature.[35]

A. Degradation process

The degradation process of undoped and Fe-doped $SrTiO_3$ is illustrated in Fig. 3 by plotting the real part of admittance (conductance) Y' as a function of time and several $M''(f)$ spectra at selected degradation times. The plot of

conductance as a function of time demonstrates the increase of effective conductivity in the dielectrics which leads to a stable degraded state. These plots are equivalent to the typically shown current density vs. time plots, since both quantities are proportional at low frequencies. Undoped $SrTiO_3$ exhibits a greater increase in conductivity than Fe-doped $SrTiO_3$, even at a lower electric field strength.

The plots of $M''(f)$ spectra at selected degradation times, reveal the impact of field stress on the changes in conductivity. Degradation of Fe-doped $SrTiO_3$ is characterized by the formation of two differently conductive anode and cathode regions, which results in two separated $M''(f)$ peaks. The height of the peak is proportional to the size of the respective region. It has been demonstrated that the smaller low frequency peak is related to the lower conductive and smaller anode region.[13] The second peak is related to the more conductive cathode region. The temporal change in conductance of each region can be monitored separately by choosing suitable frequencies. A low frequency value $Y'(f = 200\,\text{Hz})$ is dominated by the anode region, while a frequency in between both $M''(f)$ peaks, such as $Y'(f = 70\,\text{kHz})$, reflects the cathode properties. As shown in Fig. 3(a), both regions exhibit a stable degraded state.

Undoped $SrTiO_3$ on the other hand does not split into two peaks during degradation. There is only a slight decrease in peak height observed, which can be related to a broadening of the conductivity distribution. Degradation of undoped $SrTiO_3$ with different dielectric thicknesses and similar applied electrical field is also compared. Surprisingly, the thicker sample exhibits a higher increase in conductivity due to field stress. In addition, the degradation time does not scale with the distance between the electrodes, which is observed for acceptor doped $SrTiO_3$,[12] but is rather independent of the dielectric thickness. It also needs to be pointed out that Fe-doped and nominally undoped $SrTiO_3$ exhibit similar impurity concentrations. Utilizing laser ablation inductively coupled plasma mass spectroscopy, all impurity levels are found below 5 ppm except for Ba (~30 ppm) which is, however, isovalent with Sr. The changes in the electrical properties of Fe-doped $SrTiO_3$ compared to undoped $SrTiO_3$, are thus primarily due to the intentional doping with iron.

B. Temperature dependent properties of the degraded state

Subsequent to establishing the stable degraded condition, the temperature is gradually decreased in 10 °C steps, while the dc voltage is kept on. Figure 4 illustrates the $M''(f)$ spectra for selected temperatures, as well as the respective distribution of conductivity. To obtain the distribution of conductivity, a least squares fit of the real and imaginary part of the modulus is employed.[22] For this purpose, the sample is matched with a 1-dimensional equivalent circuit model of 100 equally sized slices.[22] For example, each virtual slice of a sample with 3 mm thickness represents a region within the sample with a size of 30 μm. The slices are represented by an ideal RC element, that all exhibit a constant permittivity, while each conductivity value is fitted simultaneously. The details of this procedure are given elsewhere.[22] The fit of the impedance data, however, does not contain information regarding spatial ordering, so that the conductivity values are plotted in the ascending order.

The $M''(f)$ spectra of Fe-doped $SrTiO_3$ shift to lower frequencies with decreasing temperature. Both modulus peak heights decrease since the permittivity of $SrTiO_3$ increases with decreasing temperature. The distance between both peaks, as well as the ratio of both peak heights, however, are independent of temperature so that the size of both regions does not change with temperature. The distribution of conductivity determined by fitting reflects this observation. Moreover, it is apparent that there is no distribution of conductivity in the lower conductive anode region, while conductivity varies by about one order of magnitude in the cathode region. The oxygen vacancy concentration in the cathode region is expected to continuously increase from the coloration front to the electrode interface. Inevitably, the electron concentration is characterized by the same trend so that the profile shown in Fig. 4(d) is very likely the actual distribution of conductivity in the crystal with slice [100] representing the cathode electrode interface.

Degraded, undoped $SrTiO_3$ with planar electrodes is characterized by one peak shifting to lower frequencies with decreasing temperature. Similar to Fe-doped $SrTiO_3$, the peak height decreases due to an increasing permittivity and the range of conductivity values is about two orders of magnitude. However, undoped $SrTiO_3$ is characterized by a significantly different conductivity distribution such that only one modulus peak is observed. With planar electrodes, the conductivity distribution does not change as a function of temperature. On the contrary, degraded undoped $SrTiO_3$ with lateral electrodes exhibits drastic changes in conductivity distribution as a function of temperature. Some regions exhibit a weak temperature dependence, while others show a strong dependence, which leads to a splitting of one to two peaks with decreasing temperature. This behavior has been observed on a multitude of undoped samples with lateral electrodes. Currently, there is no complete model that could describe the degradation behavior of undoped $SrTiO_3$, which is why it is very important to study this behavior in more detail. First of all, it is necessary to evaluate the temperature dependence of conductivity.

The temperature dependence of the conductivity may be described by an Arrhenius type behavior with

$$\sigma = \sigma_0 \exp\left(-\frac{E_A}{k_B T}\right), \tag{2}$$

where σ_0 is the pre-exponential factor, k_B is the Boltzmann constant, T is the temperature, and E_A is the activation energy. There are two approaches to obtain the conductivity values to determine E_A of the data shown in Fig. 4. Either conductivity is calculated using Eq. (1) and the peak maxima of M'' or the fitted distribution of conductivity is utilized so that each slice can be analyzed separately.

The use of Eq. (1) allows determination of the average conductivity in each region. It is only applicable if the $M''(f)$ spectra are characterized by one peak or if the respective

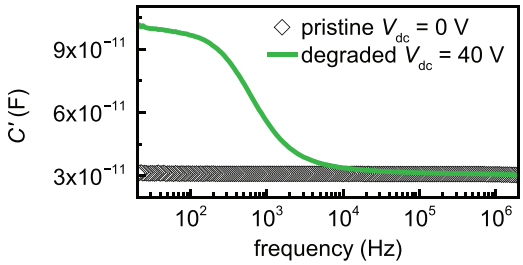

FIG. 5. Comparison of real part of the capacitance $C'(f)$ for the pristine and degraded state of Fe-doped $SrTiO_3$ at 132 °C. The high frequency part indicates that the relative permittivity does not change with the application of $V_{dc} = 40$ V.

peaks are considerably far apart. Consequently, this method cannot be used for degraded undoped $SrTiO_3$ with lateral electrodes. It is important to note that the permittivity used for this method needs to be determined at frequencies high enough so that space charge effects do not affect the capacitance measurement. In case this is not possible, the permittivity value of the pristine state which is not strongly impaired by space charges may be used. Especially for $SrTiO_3$ single crystals, this is applicable as the applied field is low and the permittivity is not altered by soft mode hardening effects. As an example, Fig. 5 illustrates the real part of the capacitance *C'* as a function of frequency. *C'* at high frequencies and fixed temperature is not altered due to degradation. The values of ε_r as well as f_r and σ in the anode and cathode region of degraded Fe-doped $SrTiO_3$ are given in Table I. The plots in Fig. 6 demonstrate that the conductivity follows an Arrhenius behavior. The activation energy of degraded Fe-doped $SrTiO_3$ is 1.00 ± 0.02 eV and 1.01 ± 0.02 eV in the anode and cathode region, respectively. For degraded, undoped $SrTiO_3$, an activation energy of 0.63 ± 0.02 eV is determined.

Alternatively, the activation energy of conductivity may be determined within any slice of the crystal. At this point, it needs to be recalled that the oxygen vacancy profile of the degraded state is time invariant. In addition, trends in temperature dependent changes of local conductivity are expected to be homogeneous. Thus, a specific slice is not expected to change position as long as the type of ordering, which is here in any case ascending, is not altered. However, precise fitting of the conductivity distribution within the crystal is inevitable,

TABLE I. Summary of relative permittivity ε_r, as well as relaxation frequency f_r and conductivity of the anode and cathode region for Fe-doped $SrTiO_3$ in the degraded state. The absolute error of the temperature is ±1 °C, while the other quantities exhibit a relative error of 7% (ε_r), 3% (f_r), and 10% (σ).

T (°C)	ε_r ()	$f_{r,\,anode}$ (Hz)	$f_{r,\,cathode}$ (Hz)	σ_{anode} (Scm^{-1})	$\sigma_{cathode}$ (Scm^{-1})
211	227	8.43×10^3	3.17×10^5	1.1×10^{-6}	4.0×10^{-5}
201	231	4.74×10^3	1.89×10^5	6.1×10^{-7}	2.4×10^{-5}
191	235	2.83×10^3	1.06×10^5	3.7×10^{-7}	1.4×10^{-5}
182	240	1.50×10^3	5.97×10^4	2.0×10^{-7}	8.0×10^{-6}
172	245	8.43×10^2	3.36×10^4	1.2×10^{-7}	4.6×10^{-6}
162	250	4.48×10^2	1.89×10^4	6.2×10^{-8}	2.6×10^{-6}
152	255	2.38×10^2	9.46×10^3	3.4×10^{-8}	1.3×10^{-6}
142	261	1.26×10^2	4.74×10^3	1.8×10^{-8}	6.9×10^{-7}
132	267	6.33×10^1	2.24×10^3	9.4×10^{-9}	3.3×10^{-7}

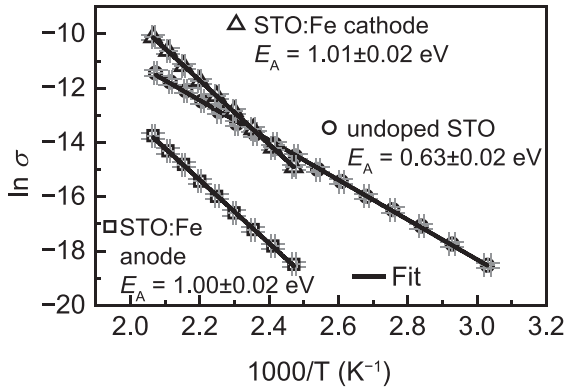

FIG. 6. Arrhenius plot of degraded Fe-doped and undoped $SrTiO_3$ with the planar geometry. The conductivity values are determined by the peak position f_r of each M'' peak.

which implies time-consuming fitting procedures. The determined activation energy in each slice in conjunction with the standard deviation is presented in Fig. 7. The basis for this fit is the data given in Fig. 4. Degraded Fe-doped $SrTiO_3$ exhibits an activation energy of 1.04 ± 0.03 eV in the anode region, which is constant similar to the conductivity in this region. The cathode region (slices 30–95) is characterized by an average activation energy of 0.99 ± 0.09 eV with slight scattering which might be related to the precision of fitting the conductivity distribution. Close to the cathode electrode interface, the activation energy significantly decreases. The average activation energy of degraded undoped $SrTiO_3$ with planar electrodes is 0.65 ± 0.2 eV. In this case, scattering is strong and might be related to the broad conductivity distribution of two orders of magnitude which is difficult to fit accurately. Degraded undoped $SrTiO_3$ with lateral electrodes exhibits a transition between two different activation energies. The emerging low frequency peak is characterized by an activation energy of 0.63 ± 0.02 eV, while the high frequency peak exhibits an activation energy of 0.15 ± 0.05 eV.

IV. DISCUSSION

The use of in-situ impedance to study the degradation process of undoped and Fe-doped $SrTiO_3$ has revealed crucial differences in spatio-temporal changes of conductivity. Fe-doped $SrTiO_3$ forms two separate $M''(f)$ peaks which can

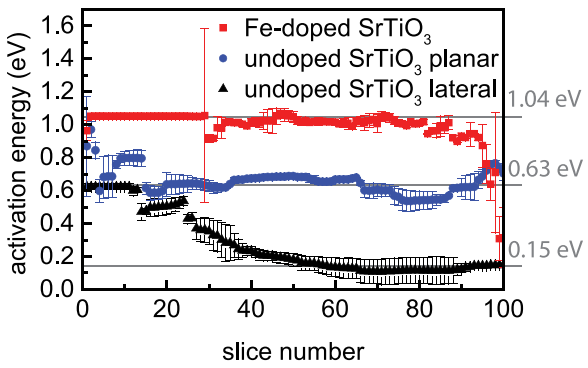

FIG. 7. Plot of activation energy for each slice within the sample, which is determined from the temperature dependent conductivity data presented in Fig. 4.

be understood with current theories,[12,13,29] while undoped $SrTiO_3$ sustains one $M''(f)$ peak throughout the degradation. Even though the peak shape is crucially different, the interval in which conductivity values are found is with 2 (undoped) and 2.5 (Fe-doped) orders of magnitude similar. For undoped $SrTiO_3$, the degradation time does not scale with the dielectric thickness which suggests that oxygen vacancy migration is not the limiting mechanism for degradation. Presumably, electric field driven processes such as charge injection are involved here.[38] To highlight the different ways the modulus feature may change during degradation, a simple terminology is proposed which indicates the number of modulus peaks at different stages of degradation. The first number indicates the pristine state, while the last number indicates the degraded state. In this case, Fe-doped $SrTiO_3$ is of (1–2) type and undoped $SrTiO_3$ is of (1–1) type. Degradation characterized by only one $M''(f)$ peak and thus (1–1) type was also found for Mg-doped $SrTiO_3$[26] ceramics and Fe-doped $BaTiO_3$[23] single crystals. However, up to now, there is no published model that could explain the observed behavior since oxygen vacancy migration is always expected to result in an oxygen vacancy poor and an oxygen vacancy rich region with different conductivities. There is also a third variation found for Mg-doped $BaTiO_3$ which shows the transition from one to two and back to one $M''(f)$ peak (1-2-1).[39] It turns out that the degradation behavior of mixed ionic conductors can be classified based on the number of modulus peaks observed during degradation. Currently, the types (1-1), (1-2), or (1-2-1) are known, but further categories may exist. The type of category a material belongs to evidently depends on the dominant impurity type and its relevant defect position within the band gap. When comparing the above-mentioned material systems, only the defect levels of Fe in $SrTiO_3$ appear to be suitable to form both a stable hole dominated anode region and a stable electron dominated cathode region.

The evaluation of the temperature dependent conductivity of the degraded state was carried out with conductivity values obtained by the modulus peak position and fitted conductivity values in respective slices. Both approaches resulted in comparable activation energies. The latter results in a higher scattering of the activation energy value due to the required high precision of fitting the conductivity distribution. However, this process allows to gain information about samples that are not characterized by modulus peaks that are unambiguous to determine. This is in particular, valuable for degraded undoped $SrTiO_3$ with lateral electrodes. Two regions with different activation energies were identified. One region exhibits a low activation energy of 0.15 eV. This value is close to 0.1 eV, often found for small polaron conduction[40–42] and suggests a strong impact of Ti^{3+} states on the charge transport. The other region is characterized by an activation energy of 0.62 eV, which reflects the properties of degraded undoped $SrTiO_3$ with planar electrodes. More importantly, the value of 0.62 eV is identical with the activation energy of the pristine state, which suggests that oxygen vacancies also play a crucial role in charge transport of the degraded state. However, a major contribution of oxygen vacancies in the degraded state is excluded since the established time invariant conductive state suggests no further migration of ionic species. Moreover, two orders of magnitude higher conductivity in the entire degraded sample would require an increase of the total oxygen vacancy concentration of two orders of magnitude which is also unreasonable. Most likely, the similarity of activation energy for oxygen vacancy migration and the degraded state of undoped $SrTiO_3$ is only a coincidence and the true origin of charge transport in the degraded state is currently unknown. To understand both, the activation energy of 0.15 eV and 0.62 eV of the degraded state, further investigations will be necessary. However, detection of these former unknown activation energies illustrates the importance of in-situ impedance studies with applied dc voltage to unravel the mechanism dominating the degraded state. This is particularly important since there are many indicators that field driven oxygen vacancy migration alters the properties of mixed ionic conductors which are not implemented in modeling efforts. Possible consequences are the dissociation of defect complexes that exist in the pristine state,[35,43–45] charge injection due to Schottky barrier lowering,[38,46] local strain,[30,47–50] and formation of additional defect types such as Jahn-Teller distortions in the anode region,[30,51] and reduction of titanium in the cathode region.[25,46,52]

Finally, the specific case of degraded Fe-doped $SrTiO_3$ illustrated in Fig. 1 is discussed. Using in-situ impedance studies with applied dc voltage, an activation energy of 1.00 eV is determined in the anode region. This is in very good agreement with earlier studies utilizing polarization experiments which found an activation energy of 1.01 eV in the respective temperature range.[21]

The magnitude of conductivity in the cathode region of degraded Fe-doped $SrTiO_3$ obtained by in-situ impedance studies with applied dc voltage, however, is significantly lower than expected by equilibrium state studies. This suggests that not all electrons that are necessary to compensate the oxygen vacancies in the cathode region can be found in the conduction band where they are free to move. Temperature dependence of conductivity is not phonon controlled, but shows a rather strong increase with increasing temperature which suggests the existence of an additional defect level. The determined activation energy is 1.01 eV which is very close to the one found in the anode region. However, the origin is expected to be different since the coloration front which separates the anode and cathode region implies a distinct change in the Fe^{3+}/Fe^{4+} ratio, which indicates a change in Fermi energy. The most reasonable explanation is that the activation energy of the anode region refers to the distance of a defect level (Fe^{3+}/Fe^{4+}) to the valence band, while the activation energy of the cathode region corresponds to the distance to the conduction band. Up to now, there is no report in the literature about the second type of defect. It is, however, very likely that the defect responsible for the activation energy in the cathode region is linked to the existence of iron in $SrTiO_3$ since the activation energy of degraded undoped and Fe-doped $SrTiO_3$ differs considerably. Options could be the reduction of iron to Fe^{2+} or a possible Fe related defect complex.[53–56]

Utilizing the acceptor levels presented above, a new set of equations can be compiled to obtain the equilibrium Fermi level position and concentration of charged defects as a function of oxygen vacancy concentration. The product of electron and hole concentrations is calculated via the band gap E_g and density of states in the conduction and valence band. In addition, charge neutrality is presumed. It is assumed that the concentration of all defects is fixed and charge states can only vary depending on the Fermi level position. The charged defect concentration is determined by

$$N_{Ai}^{-} = N_{Ai} \frac{1}{1 + g_A \exp\left(\frac{E_{Ai} - E_F}{k_B T}\right)}, \quad (3)$$

where $g_A = 4$ describes the ground-state degeneracy factor for acceptor levels,[57] $N_{A1} = N_{A2} = [\mathrm{Fe}]$, $E_{A1} = 1.00\,\mathrm{eV}$, and $E_{A2} = E_g - 1.01\,\mathrm{eV}$. The results are shown in Fig. 8 with an emphasis on the cathode region since the anode region has already been shown to match. The above model considers oxygen vacancies and electrons and holes in the conduction and valence band as conductive. These type of electrons and holes are indicated as n_{free} and p_{free}. Considering only electrons in the conduction band, the electronic conductivity falls below the oxygen vacancy conductivity. Alternatively, the contribution of the electrons n_{trap} trapped by the defect $\sim$1 eV below the conduction band may be included by a hopping process with $\mu = 4.5 \times 10^6 \exp(-1.01\,\mathrm{eV}/k_B T)\ \mathrm{cm^2\,V^{-1}\,s^{-1}}$. Thus, the hopping mobility at the degradation temperature $\mu\ (T = 210\,^\circ\mathrm{C}) = 1.3 \times 10^{-4}\ \mathrm{cm^2\,V^{-1}\,s^{-1}}$ is significantly lower than the free mobility, but due to the considerably higher charge carrier density the measured conductivity is matched. It is therefore proposed that trapped charges characterized by a hopping mobility define the conductivity of the cathode region. The model fits the temperature dependent conductivity as shown in Fig. 8. Modeling of the degradation process with the new defect set will be presented separately. It needs to be mentioned that the possibility remains that the assumption of two fixed defect states is still too simplistic, and in fact, an ensemble of impurities, and their respective concentration and defect level position need to be considered. Irrespective of that, the model mentioned above is the first one to describe the conductivity of Fe-doped $SrTiO_3$ within the entire degraded crystal.

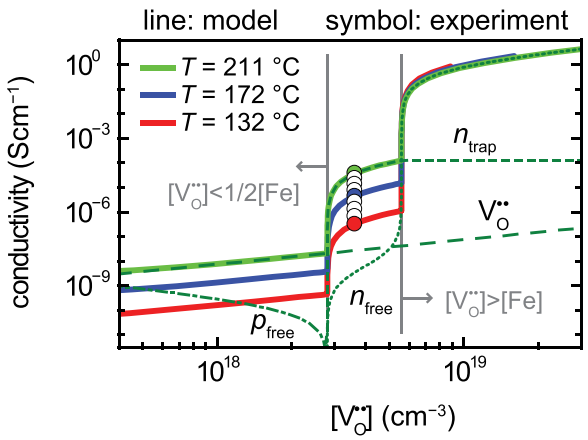

FIG. 8. Plot of conductivity as a function of oxygen vacancy concentration that considers an additional defect contribution in the cathode region.

V. CONCLUSION

The method of in-situ impedance studies with applied dc voltage permits the study of the distribution of local conductivity during degradation and at the degraded state as a function of temperature. In particular, the application of a dc voltage during the investigation reflects the conditions of a device in use and field driven effects that can be incorporated into the analysis. The degradation process of undoped and Fe-doped $SrTiO_3$ revealed crucial differences in the local conductivity distribution visible by the number of modulus peaks. Fe-doped $SrTiO_3$ belongs to the type (1-2) which shows a splitting of one peak into two peaks. Undoped $SrTiO_3$, however, belongs to the more common (1-1) type which does not show peak splitting. It is expected that classification of various materials into different types will allow to study degradation more systematically in future.

Two approaches have been presented to determine the activation energy of degraded $SrTiO_3$. The activation energy of degraded Fe-doped $SrTiO_3$ in the anode region confirmed the findings of earlier studies, while the following activation energies have been determined for the first time. The cathode region of degraded Fe-doped $SrTiO_3$ exhibits an activation energy of 1.01 eV and the new defect model based on an additional acceptor type trap has been presented. In degraded, undoped $SrTiO_3$, activation energies of 0.63 eV and 0.15 eV are found. The latter suggests a major contribution of Ti^{3+} to charge carrier transport, while the former clarifies that charge transport in degraded, undoped $SrTiO_3$ is crucially different to degraded Fe-doped $SrTiO_3$. It is anticipated that expanding the analysis to a wider range of materials will advance the understanding of resistance degradation mechanisms considerably.

ACKNOWLEDGMENTS

The authors gratefully acknowledge financial support for this work provided by the AFOSR Grant Nos. FA9550-14-1-0067 (T.J.M.B., J.J.C., and C.A.R.), FA9550-14-1-0264 (J.J.W. and L.Q.C.), and FA9550-14-1-0158 (A.K.) (Program manager: Ali Sayir).

[1]M.-J. Pan and C. A. Randall, Electr. Insul. Mag. IEEE **26**, 44 (2010).
[2]H. Kishi, Y. Mizuno, and H. Chazono, Jpn. J. Appl. Phys. **42**, 1 (2003).
[3]J. Rödel, K. G. Webber, R. Dittmer, W. Jo, M. Kimura, and D. Damjanovic, J. Eur. Ceram. Soc. **35**, 1659 (2015).
[4]S. Zhao, S. J. Zhang, W. Liu, N. J. Donnelly, Z. Xu, and C. A. Randall, J. Appl. Phys. **105**, 53705 (2009).
[5]R. Waser, T. Baiatu, and K.-H. Härdtl, J. Am. Ceram. Soc. **73**, 1654 (1990).
[6]Y. A. Genenko, J. Glaum, M. J. Hoffmann, and K. Albe, Mater. Sci. Eng. B Solid-State Mater. Adv. Technol. **192**, 52 (2015).
[7]J. Watson and G. Castro, J. Mater. Sci. Mater. Electron. **26**, 9226 (2015).
[8]H. Chazono and H. Kishi, Jpn. J. Appl. Phys. **40**, 5624 (2001).
[9]C. A. Randall, R. Maier, W. Qu, K. Kobayashi, K. Morita, Y. Mizuno, N. Inoue, and T. Oguni, J. Appl. Phys. **113**, 14101 (2013).
[10]R. G. Polcawich, C.-N. Feng, S. Kurtz, S. Perini, P. J. Moses, and S. Trolier-McKinstry, The International Journal of Microcircuits and Electronic Packaging **23**, 85–91 (2000); available at http://www.imaps.org/journal/2000/Q1/polcawich12.pdf.
[11]N. J. Donnelly and C. A. Randall, J. Am. Ceram. Soc. **92**, 405 (2009).

[12]T. Baiatu, R. Waser, and K.-H. Härdtl, J. Am. Ceram. Soc. **73**, 1663 (1990).
[13]T. J. M. Bayer, J.-J. Wang, J. J. Carter, A. Moballegh, J. Baker, D. L. Irving, E. C. Dickey, L.-Q. Chen, and C. A. Randall, Acta Mater. **117**, 252 (2016).
[14]R. Waser and R. Hagenbeck, Acta Mater. **48**, 797 (2000).
[15]R. Waser, J. Am. Ceram. Soc. **74**, 1934 (1991).
[16]K. D. Becker, M. Schrader, H. S. Kwon, and H. I. Yoo, Phys. Chem. Chem. Phys. **11**, 3082 (2009).
[17]H. I. Yoo, T. S. Oh, H. S. Kwon, D. K. Shin, and J. S. Lee, Phys. Chem. Chem. Phys. **11**, 3115 (2009).
[18]R. Merkle and J. Maier, Angew. Chem. Int. Ed. **47**, 3874 (2008).
[19]N.-H. Chan, R. K. Sharma, and D. M. Smyth, J. Electrochem. Soc. **128**, 1762 (1981).
[20]R. Moos and K. H. Härdtl, J. Am. Ceram. Soc. **80**, 2549 (1997).
[21]I. Denk, W. Münch, and J. Maier, J. Am. Ceram. Soc. **78**, 3265 (1995).
[22]T. J. M. Bayer, J. Wang, J. J. Carter, L. Chen, and C. A. Randall, in *2016 Joint IEEE International Symposium on the Applications of Ferroelectrics, European Conference on Application of Polar Dielectrics* (IEEE, 2016), pp. 1–4.
[23]J. J. Carter, T. J. M. Bayer, and C. A. Randall, J. Appl. Phys. **121**, 145106 (2017).
[24]S. Rodewald, J. Fleig, and J. Maier, J. Am. Ceram. Soc. **83**, 1969 (2000).
[25]W. Liu, G. Y. Yang, and C. A. Randall, Jpn. J. Appl. Phys. **48**, 51404 (2009).
[26]L. G. Escrig, M. Prades, H. Beltran, E. Cordoncillo, N. Maso, and A. R. West, J. Am. Ceram. Soc. **97**, 2815 (2014).
[27]W. Liu and C. A. Randall, J. Am. Ceram. Soc. **91**, 3245 (2008).
[28]R. M. Waser, J. Am. Ceram. Soc. **72**, 2234 (1989).
[29]J.-J. Wang, H.-B. Huang, T. J. M. Bayer, A. Moballegh, Y. Cao, A. Klein, E. C. Dickey, D. L. Irving, C. A. Randall, and L.-Q. Chen, Acta Mater. **108**, 229 (2016).
[30]C. Lenser, A. Kalinko, A. Kuzmin, D. Berzins, J. Purans, K. Szot, R. Waser, and R. Dittmann, Phys. Chem. Chem. Phys. **13**, 20779 (2011).
[31]R. Moos, W. Menesklou, and K. H. Härdtl, Appl. Phys. A **61**, 389 (1995).
[32]M. Fleischer, H. Meixner, and C. Tragut, J. Am. Ceram. Soc. **75**, 1666 (1992).
[33]S. Ohta and H. Ohta, J. Appl. Phys. **97**, 34106 (2005).
[34]T. Okamoto, J. Long, R. H. T. Wilke, J. Stitt, R. Maier, and C. A. Randall, Jpn. J. Appl. Phys. **55**, 26601 (2016).
[35]R. A. Maier and C. A. Randall, J. Am. Ceram. Soc. **99**, 3350 (2016).
[36]R. A. Maier and C. A. Randall, J. Am. Ceram. Soc. **99**, 3360 (2016).
[37]J. Jamnik, J. Maier, and S. Pejovnik, Electrochim. Acta **44**, 4139 (1999).
[38]J.-J. Wang, T. J. M. Bayer, R. Wang, J. J. Carter, C. A. Randall, and L.-Q. Chen, Appl. Phys. Lett. **110**, 262902 (2017).
[39]M. Prades, N. Masó, H. Beltrán, E. Cordoncillo, and A. R. West, J. Mater. Chem. **20**, 5335 (2010).
[40]C. Gillot, J. Michenaud, M. Maglione, and B. Jannot, Solid State Commun. **84**, 1033 (1992).
[41]A. L. Shluger and A. M. Stoneham, J. Phys.: Condens. Matter **5**, 3049 (1993).
[42]E. Iguchi, N. Kubota, T. Nakamori, N. Yamamoto, and K. J. Lee, Phys. Rev. B **43**, 8646 (1991).
[43]J. N. Baker, P. C. Bowes, D. M. Long, A. Moballegh, J. S. Harris, E. C. Dickey, and D. L. Irving, Appl. Phys. Lett. **110**, 122903 (2017).
[44]M. Schie, R. Waser, and R. A. De Souza, J. Phys. Chem. C **118**, 15185 (2014).
[45]R. A. Maier, T. A. Pomorski, P. M. Lenahan, and C. A. Randall, J. Appl. Phys. **118**, 164102 (2015).
[46]R. Giesecke, R. Hertwig, T. J. M. Bayer, C. A. Randall, and A. Klein, J. Am. Ceram. Soc. **100**, 4590–4601(2017).
[47]D. Ascienzo, S. Greenbaum, T. J. M. Bayer, C. A. Randall, and Y. H. Ren, Acta Mater. **126**, 520 (2017).
[48]D. Ascienzo, H. Yuan, S. Greenbaum, T. J. M. Bayer, R. A. Maier, J.-J. Wang, C. A. Randall, E. C. Dickey, H. Zhao, and Y. Ren, Materials **9**, 883 (2016).
[49]D. Ascienzo, S. Greenbaum, T. J. M. Bayer, R. Maier, C. A. Randall, and Y. H. Ren, Appl. Phys. Lett. **109**, 31602 (2016).
[50]O. Kurt, D. Ascienzo, S. Greenbaum, T. J. M. Bayer, C. A. Randall, N. Madamopoulos, and Y. H. Ren, Mater. Chem. Phys. **198**, 131 (2017).
[51]M. Vracar, A. Kuzmin, R. Merkle, J. Purans, E. A. Kotomin, J. Maier, and O. Mathon, Phys. Rev. B **76**, 174107 (2007).
[52]G. Y. Yang, G. D. Lian, E. C. Dickey, C. A. Randall, D. E. Barber, P. Pinceloup, M. A. Henderson, R. A. Hill, J. J. Beeson, and D. J. Skamser, J. Appl. Phys. **96**, 7500 (2004).
[53]C. T. Luiskutty and P. J. Ouseph, Solid State Commun. **13**, 405 (1973).
[54]V. G. Bhide and H. C. Bhasin, Phys. Rev. **172**, 290 (1968).
[55]M. Multani, Mater. Res. Bull. **19**, 25 (1984).
[56]A. Koehl, D. Kajewski, J. Kubacki, C. Lenser, R. Dittmann, P. Meuffels, K. Szot, R. Waser, and J. Szade, Phys. Chem. Chem. Phys. **15**, 8311 (2013).
[57]S. M. Sze and K. K. Ng, *Physics of Semiconductor Devices* (John Wiley & Sons, Inc., Hoboken, New Jersey, 1985).